

## OPTICAL AND DYNAMICAL CHARACTERIZATION OF COMET-LIKE MAIN-BELT ASTEROID (596) SCHEILA

HENRY H. HSIEH<sup>a,b</sup>, BIN YANG<sup>a</sup>, NADER HAGHIGHIPOUR<sup>a</sup>

<sup>a</sup>Institute for Astronomy, Univ. of Hawaii, 2680 Woodlawn Drive, Honolulu, Hawaii 96822, USA

<sup>b</sup>Hubble Fellow

Submitted, 2011-05-09; Accepted, 2011-09-14

### ABSTRACT

We present observations and a dynamical analysis of the comet-like main-belt object, (596) Scheila. *V*-band photometry obtained on UT 2010 December 12 indicates that Scheila's dust cloud has a scattering cross-section  $\sim 1.4$  times larger than that of the nucleus, corresponding to a dust mass of  $M_d \sim 3 \times 10^7$  kg. *V* – *R* color measurements indicate that both the nucleus and dust are redder than the Sun, with no significant color differences between the dust cloud's northern and southern plumes. We also undertake an ultimately unsuccessful search for CN emission, where we find CN and H<sub>2</sub>O production rates of  $Q_{\text{CN}} < 9 \times 10^{23} \text{ s}^{-1}$  and  $Q_{\text{H}_2\text{O}} < 10^{27} \text{ s}^{-1}$ . Numerical simulations indicate that Scheila is dynamically stable for  $> 100$  Myr, suggesting that it is likely native to its current location. We also find that it does not belong to a dynamical asteroid family of any significance. We consider sublimation-driven scenarios that could produce the appearance of multiple plumes of dust emission, but reject them as being physically implausible. Instead, we concur with previous studies that the unusual morphology of Scheila's dust cloud is most simply explained by a single oblique impact, meaning this object is likely not a main-belt comet, but is instead the second disrupted asteroid after P/2010 A2 (LINEAR) to be discovered.

*Subject headings:* comets: general — minor planets, asteroids

### 1. INTRODUCTION

Discovered on 1906 February 21, main-belt asteroid (596) Scheila has a diameter of  $d = 113.34$  km (Tedesco *et al.* 2004), an orbital period of  $P_{\text{orb}} = 5.01$  years, a semi-major axis of  $a = 2.927$  AU, an eccentricity of  $e = 0.165$ , an inclination of  $i = 14.66^\circ$ , and a Tisserand parameter (with respect to Jupiter) of  $T_J = 3.209$ . On 2010 December 10.4, observations by S. Larson using the 0.68 m Catalina Schmidt telescope showed that Scheila was exhibiting comet-like activity. Examination of archived Catalina data indicated that the object also appeared diffuse on December 3, but was point-source-like on October 18, November 2, and November 11 (Larson 2010).

If its activity is truly cometary, Scheila would be the newest member of the small class of objects known as main-belt comets (MBCs), which are objects that exhibit cometary activity (*e.g.*, dust emission) due to the sublimation of volatile ices, but occupy stable orbits entirely confined to the main asteroid belt (Fig. 1). MBCs are unlikely to originate in the outer solar system like other comets, and are probably native to the main belt (Fernández *et al.* 2002; Haghighipour 2009). Their activity is believed to be triggered by impacts that excavate subsurface volatile material (probably water ice; Priolnik & Rosenberg 2009; Schorghofer 2008), exposing it to direct solar heating, driving sublimation and comet-like dust emission (Hsieh & Jewitt 2006). Noting the strong correlation between activity and proximity to perihelion for all currently known MBCs, however, Hsieh *et al.* (2011b) proposed the alternate possibility that activity is in fact primarily dependent on heliocentric distance, and only peaks during the post-perihelion portion of each

MBC's orbit due to the finite time required for solar thermal waves to propagate through insulating surface material before reach the subsurface reservoirs of volatile material below. Currently, both hypotheses are consistent with the available evidence, though we note the first hypothesis could be ruled out (at least as a universally applicable explanation for MBC activity modulation) by the determination of a pole orientation for an MBC that is inconsistent with seasonal modulation of activity (*i.e.*, where peak activity does not occur near a solstice position, as required by the seasonal modulation hypothesis, but near an equinox position). Likewise, the second hypothesis could be ruled out as a universal explanation for MBC activity modulation by the discovery of an MBC which exhibits peak activity prior to reaching perihelion.

To date, gas emission has never been directly detected for an MBC (*e.g.*, Jewitt *et al.* 2009; Licandro *et al.* 2011). This present lack of spectroscopic confirmation of outgassing is largely due to the faintness of MBC activity, requiring extremely sensitive observations. Gas detection efforts are further complicated by the transience of MBC activity, requiring that spectroscopic observations be secured soon after new MBCs are discovered, something that has only been achieved for the more recent discoveries. Since rapid gas dissipation timescales mean that dust emission may continue long after active sublimation has actually ceased, even those observations may not have been sufficiently prompt to detect gas.

Despite the lack of direct gas detections, volatile sublimation is inferred to be the driver of activity for all of the objects considered to be MBCs. The indirect evidence for cometary activity typically includes observations showing recurrent activity and dust modeling showing continuous dust emission during each active episode, both con-

sistent only with sublimation-driven dust ejection (Hsieh *et al.* 2004, 2011a,b).

There is, however, the case of P/2010 A2 (LINEAR), which orbits in the main belt and exhibited a comet-like dust tail in 2010. Moreno *et al.* (2010) initially reported that numerical dust modeling indicated that the object’s apparent activity was due to emission that persisted over several months, implying that it was likely due to ice sublimation. However, follow-up modeling based on high-resolution Wide Field Camera 3 images from the Hubble Space Telescope (Jewitt *et al.* 2010) found that the apparent activity of P/2010 A2 was actually most likely a consequence of an inter-asteroid impact, rather than the product of sublimation. Observations revealed a gap between P/2010 A2’s dust tail and its nucleus, suggesting that the dust was ejected in a single burst, as would be expected from an impact-generated ejecta cloud, and was drifting away. This scenario was corroborated with further modeling by Snodgrass *et al.* (2010), who employed both ground-based data and data from the OSIRIS Narrow Angle Camera aboard the European Space Agency’s Rosetta spacecraft, and thus were able to study the dust tail from two different viewing perspectives, providing additional constraints on their model. Thus, while P/2010 A2 may have appeared comet-like, it is likely not a true comet (*i.e.*, an object that exhibits sublimation-driven activity) and is better characterized as a disrupted asteroid, that is, an object that exhibits dust emission as a consequence of an impact (or impacts), and not through the action of sublimating ice.

All studies of Scheila’s 2010 outburst published to date (Jewitt *et al.* 2011; Bodewits *et al.* 2011; Yang & Hsieh 2011; Ishiguro *et al.* 2011a,b; Moreno *et al.* 2011b) conclude that, like for P/2010 A2, Scheila’s dust cloud is likely be impact-generated, and not a consequence of sublimation. In this manuscript, we describe the results of work aimed at better understanding the full nature of Scheila and its 2010 outburst that provide additional evidence supporting this conclusion.

## 2. OBSERVATIONS

We observed Scheila on multiple occasions shortly after the discovery of its comet-like activity. Optical imaging was performed in photometric conditions on UT 2010 December 12 using the University of Hawaii (UH) 2.2 m telescope, while optical spectroscopy was obtained using the 10 m Keck I telescope on UT 2010 December 17. Details of these observations are listed in Table 1. Results of additional near-infrared observations conducted as part of this observational campaign are reported in Yang & Hsieh (2011).

Imaging observations employed a Tektronix 2048×2048 pixel CCD (0.219 pixel<sup>-1</sup>) behind Kron-Cousins filters. Spectroscopic observations were made using Keck’s Low Resolution Imaging Spectrometer (LRIS; Oke *et al.* 1995), a two-channel instrument that splits incoming light into red and blue components, and employs dual Tektronix 2048×2048 CCDs (0.135 pixel<sup>-1</sup>). We used a 1.0-wide long-slit mask, 600/4000 grism, and 560 dichroic, giving a dispersion of 0.61Å pixel<sup>-1</sup> and resolution of ~4Å.

Bias subtraction and flat-fielding were performed for UH data, where flat fields were constructed from images of the twilight sky. Photometry of Scheila’s nu-

cleus was performed using circular apertures (with background statistics measured in nearby regions of blank sky to avoid coma contamination) and calibrated using Landolt (1992) standard stars.

For our spectroscopic observations, to avoid saturation from the nucleus while still maximizing the possibility of detecting gas emission in the faint dust cloud, we used a north-south slit orientation, offset 0.6 east of the object’s photocenter. North-south dithers (by 30”) were employed to sample the sky background. We obtained two 900s exposures for a total integration time of 1800s. Bias subtraction, flat-fielding, and wavelength calibration were performed using Low-Redux<sup>1</sup> software. Object identification, extraction, and flux calibration were performed using the Image Reduction and Analysis Facility (IRAF) software package.

## 3. RESULTS & ANALYSIS

### 3.1. Photometric Analysis

We find a mean *V*-band magnitude for Scheila’s nucleus of  $m_V = 14.22 \pm 0.01$  mag inside a photometry aperture 3.0 in radius (Table 2). This measurement represents a photometric excess of  $\Delta m_V = 0.37$  mag from the quiescent magnitude ( $m_V = 14.59$  mag) predicted by Scheila’s IAU phase law ( $H_V = 8.84 \pm 0.04$ ,  $G = 0.076 \pm 0.06$ ; Warner *et al.* 2010), which significantly exceeds the amplitude of its measured rotational lightcurve (0.09 mag; Warner 2006), indicating the presence of unresolved near-nucleus coma equivalent to ~ 40% of the nucleus scattering cross-section inside the photometry aperture.

In a rectangular aperture enclosing the entire dust cloud (“A” in Figure 2), we find a total magnitude of  $m_V = 13.73 \pm 0.02$  mag, corresponding to a photometric excess of  $\Delta m_V = 0.86$  mag. The size of this rectangular aperture is chosen to encompass the entire dust cloud as observed in *V*-band before it becomes visibly indistinguishable from the background sky. However, we see in Figure 2 that the dust cloud extends somewhat farther when observed in *R*-band. Measuring the dust cloud’s *R*-band flux using a larger aperture and comparing to the flux measured using the same aperture used for our *V*-band data, we determine that the *V*-band flux of the dust cloud may be underestimated by ~ 10%, and so for the purposes of estimating the total mass of Scheila’s dust cloud, apply this offset to obtain aperture-corrected values of  $m_V = 13.63 \pm 0.02$  mag and  $\Delta m_V = 0.96$  mag. Using the nucleus for calibration, we find a total dust scattering cross section of  $A_d = (1.4 \pm 0.3) \times 10^4$  km<sup>2</sup> (~ 140% of the nucleus cross-section). Assuming a typical bulk density of  $\rho = 1640$  kg m<sup>-3</sup> (cf. the Tagish Lake meteorite; Hildebrand *et al.* 2006) and an average particle radius of  $a_d = 1 \times 10^{-6}$  m, we can estimate the total dust mass,  $M_d$ , of the cloud using

$$M_d = \frac{4}{3} A_d \rho a_d \quad (1)$$

Inserting the scattering cross-section we measure for Scheila’s dust cloud, we thus obtain an approximate dust mass of  $M_d \sim 3 \times 10^7$  kg. This estimate is of course

<sup>1</sup> Developed by J. X. Prochaska and available at <http://www.ucolick.org/~xavier/LowRedux/>

based on numerous assumptions, particularly average dust grain size and bulk density, as specified above, and is only computed to provide approximate physical context to the photometric excess that was measured. For reference, employing the different grain size distribution and density assumptions made by Jewitt *et al.* (2011) ( $\rho = 2000 \text{ kg m}^{-3}$ ;  $a_d = 1 \times 10^{-6} \text{ m}$ ) and Bodewits *et al.* (2011) ( $\rho = 2500 \text{ kg m}^{-3}$ ;  $a_d = 1 \times 10^{-4} \text{ m}$ ), we would instead obtain  $M_d \sim 4 \times 10^7 \text{ kg}$  and  $M_d \sim 5 \times 10^9 \text{ kg}$ , respectively.

For comparison, Larson (2010) measured  $\Delta m_V = 1.24 \text{ mag}$  on 2010 December 3, while Bodewits *et al.* (2011) measured  $\Delta m_V = 0.66 \text{ mag}$  on 2010 December 14–15 and Jewitt *et al.* (2011) measured  $\Delta m_V = 1.26 \text{ mag}$  on 2010 December 28 and  $\Delta m_V = 1.00 \text{ mag}$  on 2011 January 5. However, given the different observational and instrumental circumstances involved (especially given the technical difficulty of observing the extremely bright nucleus and comparatively extremely faint dust cloud simultaneously), with the exception of the decline between the two measurements by Jewitt *et al.* (2011), we do not consider any dust mass fluctuations implied by comparing these disparate data sets to be reliable.

$V - R$  color measurements (Table 2) of the dust-contaminated nucleus indicate that it is redder than the Sun, with the entire dust cloud with nucleus flux subtracted (“Dust<sub>A</sub>” in Table 2) having an effectively identical red color, similar to colors measured for other active comets and active Centaurs (Bodewits *et al.* 2011; Jewitt 2009). Assuming that the dust contaminating our nucleus photometry has a scattering cross-section 40% larger than that of the nucleus (estimated above) and the same color as the dust cloud as a whole, we find a dust-subtracted color for the nucleus of  $V - R \approx 0.44 \text{ mag}$ , consistent with a D-type spectral classification (Fornasier *et al.* 2007). To test whether the northern and southern plumes of Scheila’s dust cloud exhibit any compositional differences, we measure their colors individually (“Dust<sub>B</sub>” and “Dust<sub>C</sub>”), but within estimated uncertainties, find no significant color differences.

## 3.2. Spectroscopic Analysis

### 3.2.1. Gas Emission Search

The most sensitive probe of sublimating gas in a comet is CN emission at 3880Å. We show the spectral image of Scheila from 3700Å to 4100Å in Figure 3a. In this image, the horizontal continuum corresponds to reflected light from the nucleus. OH sky emission lines are visible as vertical bands, and dark Fraunhofer lines in the Solar spectrum and prominent Ca H (3933Å) and K (3966Å) absorption lines are also visible. In a two-dimensional spectral image, the intensity,  $I_e$ , of a cometary emission lines should be highest near the center of the continuum and gradually decrease with increasing distance from the continuum, moving in the spatial direction. No spectral features near 3880Å exhibit such behavior, and we therefore conclude that no gas is detected.

We also search for CN emission in a one-dimensional spectrum extracted from the spectral image using a  $1''.0 \times 8''.1$  rectangular aperture centered on the continuum. Sky background was measured and subtracted using flanking regions  $10''$  to  $16''$  from the nucleus. Calibration was performed using a nearby flux standard star and a solar

analog star (Fig. 3b). Shaded regions in Figures 3b and 3c indicate where CN emission is expected, but we again find no evidence of emission, consistent with work by Bodewits *et al.* (2011), Howell & Lovell (2011), and Jehin *et al.* (2011).

### 3.2.2. Gas Production Rate Computations

To estimate Scheila’s CN production rate, we remove the continuum using a scaled solar analog spectrum (Fig. 3c), which should then leave only gas emission. Standard errors in three wavelength regions in the residual spectrum (3760Å–3830Å; 3830Å–3900Å, where CN emission is expected; and 3980Å–4050Å; each 70Å in width) are  $2.7 \times 10^{-17}$ ,  $2.0 \times 10^{-17}$ , and  $1.8 \times 10^{-17} \text{ erg cm}^{-2} \text{ s}^{-1} \text{ Å}^{-1}$ , respectively (Fig. 3c). We choose  $2.7 \times 10^{-17} \text{ erg cm}^{-2} \text{ s}^{-1} \text{ Å}^{-1}$  as a conservative estimate of the uncertainty in the CN band. Since 9P/Tempel 1 observations (Meech *et al.* 2011) utilized the same instrumental settings used here, we assume that any CN band in Scheila’s spectrum will have the same profile as in 9P’s spectrum. We therefore find a peak value of any CN band of  $3 \times (2.7 \times 10^{-17} \text{ erg cm}^{-2} \text{ s}^{-1} \text{ Å}^{-1})$ , or  $\sim 8 \times 10^{-17} \text{ erg cm}^{-2} \text{ s}^{-1} \text{ Å}^{-1}$ .

We calculate the integrated CN band flux,  $f_{\text{CN}}$ , by summing the emission flux in the shaded region, obtaining  $f_{\text{CN}} = 8.8 \times 10^{-16} \text{ erg cm}^{-2} \text{ s}^{-1}$ . We then convert  $f_{\text{CN}}$  to the total number of CN molecules,  $N_{\text{CN}}$ , using

$$L_{\text{CN}} = 4\pi\Delta^2 f_{\text{CN}} \quad (2)$$

$$\log N_{\text{CN}} = \log L_{\text{CN}} + 2.0 \log r_h - \log g(l) \quad (3)$$

where  $\Delta$  and  $r_h$  are in cm and AU, respectively, and  $g(l)$  is the resonance fluorescence efficiency, which describes the number of photons scattered per second per radical, in  $\text{erg s}^{-1} \text{ molecule}^{-1}$ . During our observations, Scheila had a radial velocity of  $\dot{r}_h = 2.5 \text{ km s}^{-1}$ , for which  $g(l, r_h) = 2.7 \times 10^{-13} \text{ erg s}^{-1} \text{ molecule}^{-1}$  when the Swings effect is taken into account (Schleicher 2010). Substituting  $f_{\text{CN}} = 8.8 \times 10^{-16} \text{ erg cm}^{-2} \text{ s}^{-1}$ , we obtain  $N_{\text{CN}} = 5.33 \times 10^{26}$ .

A simple Haser (1957) model is used to derive the CN production rate,  $Q_{\text{CN}}$ , from  $N_{\text{CN}}$ , assuming isotropic outgassing, constant radial expansion of the gas coma, and a 2-step exponential decay process. We use  $l_p = 1.3 \times 10^4$  and  $l_p = 2.2 \times 10^5$  as the effective Haser scale lengths at  $r_h = 1 \text{ AU}$  (A’Hearn *et al.* 1995), and adopt a gas velocity of

$$v = 1.112 \cdot r_h^{-0.4} \text{ km s}^{-1} \quad (4)$$

(Biver *et al.* 1997). Integrating the computed spatial column density model over a rectangle  $1800 \text{ km} \times 14480 \text{ km}$  (the physical size of the extraction aperture in the sky), we find  $Q_{\text{CN}} < 9 \times 10^{23} \text{ s}^{-1}$ . Taking average ratios of species in previously observed comets ( $\log[Q_{\text{CN}}/Q_{\text{OH}}] = -2.5$ ;  $Q_{\text{OH}}/Q_{\text{H}_2\text{O}} = 90\%$ ) (A’Hearn *et al.* 1995), we estimate a water production rate of  $Q_{\text{H}_2\text{O}} < 10^{27} \text{ s}^{-1}$ . However, given the uncertainties involved in assuming ratios of comet species measured at much closer heliocentric distances remain unchanged for an object in the main asteroid belt, we regard this estimate to be precise, at best, to an order of magnitude.

### 3.3. Dynamical Analysis

To gain a more complete understanding of the circumstances surrounding Scheila’s unusual outburst, we also consider various aspects of the object’s dynamical nature. Specifically, we consider its likely origin and whether it belongs to an asteroid family.

To address the first issue, an effort motivated by the possibility that cometary objects in the asteroid belt may not necessarily originate where they are currently seen (cf. P/2008 R1 (Garradd); Jewitt *et al.* 2009), we perform numerical simulations to assess Scheila’s dynamical stability. We generate two sets of 100 test particles with Gaussian distributions in orbital element space, centered on Scheila’s JPL-tabulated osculating orbital elements, where the two sets are characterized by  $\sigma$  values equal to  $1\times$  and  $100\times$  the JPL-tabulated uncertainties for each orbital element (Fig. 4a). We then use the N-body integration package, Mercury (Chambers 1999), to integrate the orbit of each test particle forward in time for 100 Myr.

In three runs using different randomly generated sets of test particles, no objects escape from the asteroid belt, indicating that Scheila is dynamically stable over this time period, and is likely not a recent arrival from elsewhere in the main belt or the outer solar system. We note that despite the 100-fold difference in their initial dispersions, objects from both the  $1\text{-}\sigma$  and  $100\text{-}\sigma$  sets of test particles diverge to occupy similar regions of orbital element space (Fig. 4b). This divergence occurs quickly (within  $10^4$  years) and then remains approximately constant for the 100 Myr test period (Fig. 4c), with all objects remaining roughly confined to  $2.919 < a$  (AU)  $< 2.936$ ,  $0.06 < e < 0.28$ , and  $11.5^\circ < i < 18.5^\circ$ . Objects as large as Scheila in the main asteroid belt are often simply assumed to be dynamically stable, of course, but the example of the Centaur (2060) Chiron shows that it is possible for similarly large objects to occupy dynamically unstable orbits (*e.g.*, Nakamura & Yoshikawa 1993). As such, given Scheila’s unusual comet-like outburst, it is useful to have explicit confirmation (provided by our simulations) that the object is in fact dynamically stable, and is therefore unlikely to be a recently-arrived interloper from elsewhere in the solar system.

Next, given the suggestion that MBCs might be preferentially found among members of young asteroid families due to their increased likelihood of having fresh near-surface ice compared to undisturbed asteroids (Hsieh 2009), we perform a hierarchical clustering analysis (Zappalà *et al.* 1990, 1994) on proper elements for  $\sim 135,000$  asteroids from the AstDys website (<http://hamilton.dm.unipi.it/astdys/>; Knežević & Milani 2003) to search for asteroids dynamically related to Scheila. We find only six asteroids within a cutoff value of  $\delta v' = 120 \text{ m s}^{-1}$ , where commonly recognized families have tens to thousands of dynamically related members, usually within much smaller cutoff values, as shown by Nesvorný *et al.* (2005), despite the fact that their analysis was performed when far fewer asteroids were known compared to the present day. Such a small number of related asteroids indicates that Scheila likely does not belong to a family.

This conclusion is consistent with Scheila’s size: objects  $\sim 100$  km in diameter are predicted to have colli-

sional destruction timescales longer than the age of the solar system (Farinella *et al.* 1998; Bottke *et al.* 2005). Thus, any such body observed today is likely to have a primordial origin. The Vesta family, however, shows that even extremely large asteroids can be associated with families, specifically if those families were produced by large but non-catastrophic cratering impacts (Binzel & Xu 1993; Thomas *et al.* 1997). While such events will leave parent asteroids mostly intact, they would still excavate large amounts of surface material. If a parent asteroid happens to contain ice reservoirs preserved deep beneath its surface, by removing much (if not all) of the surface material previously insulating that ice against sublimation by solar heating, large cratering impacts could render that body far more susceptible to subsequent activating impacts by smaller asteroids, such as those hypothesized to have triggered activity in other MBCs (Hsieh & Jewitt 2006). The insignificant number of asteroids found to be dynamically related to Scheila indicates, however, that not only is Scheila unlikely to be a recently-produced fragment of a larger asteroid, it is also unlikely to have experienced a large (fragment-producing) but non-catastrophic cratering impact in the recent past, and so we conclude that its likelihood of having recently exposed preserved icy material from its deep interior (*i.e.*, several km or more below its surface) is low.

## 4. DISCUSSION

### 4.1. Scheila’s Physical Nature

Yang & Hsieh (2011) found that Scheila’s near-infrared spectrum (from 0.8 to 4.0  $\mu\text{m}$ ) exhibits a consistent red slope, has no apparent absorption features, and generally resembles spectra of D-type asteroids. Using an intimate mixing model incorporating water ice, amorphous carbon, and iron-rich pyroxene, they were able to reproduce Scheila’s spectrum except for a clearly visible water absorption feature that is present in the synthetic spectrum but not the observed spectrum. Despite the absence of unambiguous evidence of water ice in these observations, given the signal-to-noise ratio of the data, Yang & Hsieh (2011) concluded that the presence of water ice on Scheila’s surface could not be excluded to a level of a few percent. They further noted that the similarity between Scheila and D-type asteroids, which in turn have been noted for their similarities to classical cometary nuclei from the outer solar system (Fitzsimmons *et al.* 1994), suggests that Scheila could contain preserved ice deep within its interior (*e.g.*, Jones *et al.* 1990).

For comparison, two other MBCs, 133P/Elst-Pizarro and 176P/LINEAR, have been identified as B-type or F-type asteroids (Bagnulo *et al.* 2010; Licandro *et al.* 2011), where both types are subgroups of C-type asteroids. Interestingly, these spectral classifications mean that, unlike Scheila, they are more physically similar to nearby main-belt asteroids than to classical comets (Licandro *et al.* 2011), even though we believe the active episodes for these objects were actually sublimation-driven in nature, while Scheila’s was not. The nuclei of MBCs 238P/Read, P/Garradd, and P/2010 R2 (La Sagra), as well as that of P/2010 A2, have yet to be characterized spectroscopically due to the small sizes of 238P and P/2010 A2 (Hsieh *et al.* 2011b; Jewitt *et al.* 2010) and significant cometary

activity at the time of all currently published observations of P/Garradd and P/La Sagra (Jewitt *et al.* 2009; Moreno *et al.* 2011a).

As discussed above (Section 1), direct spectroscopic detections of gas emission in MBCs have been elusive (*e.g.*, Jewitt *et al.* 2009; Licandro *et al.* 2011). Successful unambiguous detections of ice have been likewise difficult to obtain. No spectroscopic evidence of exposed water ice has been found on any of the MBCs (*e.g.*, Rousselot *et al.* 2011). However, Hsieh & Jewitt (2006) hypothesize that cometary activity for these objects is being driven by small areas of exposed subsurface ice (hundreds of square meters on km-sized bodies; cf. Hsieh *et al.* 2004; Hsieh 2009). If that approximate ratio of active to inactive surface material is correct, we would actually expect unresolved disk-integrated reflectance spectroscopy to be of limited use without sensitivity levels to one part in  $\sim 10^4$  or better.

While this sensitivity level is beyond the reach of current Earth-bound facilities for the km-scale (and smaller) MBCs at the distance of the asteroid belt, Rivkin & Emery (2010) and Campins *et al.* (2010) have reported water ice detections (corresponding to much larger surface coverage than predicted for the MBCs) for the 100-km-scale asteroid (24) Themis, which belongs to the same Themis asteroid family that also contains 133P and 176P (Hsieh & Jewitt 2006). A similar absorption feature has also been detected on outer belt asteroid (65) Cybele (Licandro *et al.* 2011). The attribution of the absorption feature observed by these groups to water ice has been challenged by Beck *et al.* (2011) though, who suggest that the absorption feature can be equally well explained by the non-volatile mineral goethite. Rivkin & Emery (2010) and Campins *et al.* (2010) acknowledge the thermal instability of water ice that they claim to detect and propose various scenarios how such surface ice could be maintained. However, none of these scenarios has yet been confirmed to actually plausibly account for a widespread, long-lived surface layer of water ice as implied by their observations. We further note that no outgassing or dust emission has ever been observed for (24) Themis (also noted by Rivkin & Emery 2010), and as such, the connection between ice on main-belt asteroids and the activity of MBCs remains unsubstantiated.

In summary, while the hypothesis that activity in MBCs is sublimation-driven is supported by indirect evidence such as numerical modeling results and observations showing recurrent activity (*e.g.*, Hsieh *et al.* 2009, 2010, 2011b), it remains unsubstantiated by the unambiguous detection of either ice or sublimation products. As such, if the non-detections of ice or gas emission via spectroscopy currently do not preclude the designation of an object as an MBC, the same non-detections of ice and gas emission for Scheila (Section 3.2; Howell & Lovell 2011; Jehin *et al.* 2011; Bodewits *et al.* 2011; Yang & Hsieh 2011) necessarily must also be considered inadequate criteria for concluding that the object is a disrupted asteroid, at least on their own. We must also consider other evidence.

#### 4.2. Morphology Analysis and Outburst Scenarios

The most obvious aspect of Scheila’s dust cloud that should bear clues as to its origin is its unusual morphology. Unlike many other comets which typically exhibit

a single tail, often pointed in the antisolar direction, and a coma, Scheila exhibits two distinct curved dust plumes extending to the North and the South (Figure 2). Deeper and higher resolution imagery also shows a faint westward-pointing dust “spike” (Jewitt *et al.* 2011). The two main dust plumes are not easily explained by the standard cometary dust ejection paradigm where grains are ejected isotropically and subsequently follow well-defined syndyne and synchronic curves (*cf.* Finson & Probst 1968), and therefore suggest the action of a more unusual ejection mechanism.

Ishiguro *et al.* (2011b) present numerical modeling results that show that the cloud’s morphology can be accounted for by a hollow cone of dust (as expected from an impact; *e.g.*, Richardson *et al.* 2007) ejected Sunward and then turned back by radiation pressure. The hollowness of the cone is suggested by the dust cloud’s apparent limb brightening (*i.e.*, Scheila’s northern and southern plumes), consistent with the greater optical depth expected of such a structure along its edges. A solid cone of ejected dust (as expected from a sublimation-driven jet) similarly pushed back would instead exhibit central brightening due to greater optical depth in the jet’s core, and not appear to exhibit multiple plumes. The disparate strengths of the northern and southern plumes may indicate an oblique angle of incidence for the impact, with more dust expected downrange of the inbound impactor (*cf.* Ishiguro *et al.* 2011b).

While the scenario modeled by Ishiguro *et al.* (2011b) plausibly accounts for the appearance of multiple dust plumes with a single impact, if Scheila’s dust cloud is produced by a sublimation-driven process, any scenario that similarly accounts for multiple observed dust plumes likely requires multiple active sites. If these active sites are collisionally excavated, multiple impacts would have to have occurred on timescales shorter than their depletion timescales. This scenario is unlikely, however, given the typically low rate of impacts on any single body in the asteroid belt (*e.g.*, Farinella & Davis 1992) and the expected short depletion timescales for surface volatiles on main-belt asteroids (Hsieh 2009). Multiple active sites could be possible if near-surface ice is abundant, triggering sublimation at multiple points via thermal stresses. This scenario is contradicted though by Scheila’s history of observed inactivity until 2010, and the fact that it first exhibited a comet-like dust cloud at  $\nu \sim 240^\circ$ , well before perihelion, when the surface was receiving only  $\sim 60\%$  of the solar flux that it would at perihelion. If Scheila were particularly icy, we would expect to have observed past activity and at times of maximum solar heating. We therefore find any scenario invoking multiple sublimation sites to be implausible.

One possible scenario which could explain the observed dust morphology via a sublimation-driven phenomenon would be one in which directed dust emission (*i.e.*, a jet) is being produced from a single active site near the rotational pole of the object, which in turn is directed approximately Sunward. Such a situation would mimic the effect of a hollow cone of material (*i.e.*, the rotating jet) being ejected Sunward, where the cone would then be expected to be pushed back by radiation pressure as in the impact-driven model described by Ishiguro *et al.* (2011b). Asymmetry in the density of material forming the cone could then be caused by diurnal effects where

sublimation, and therefore dust emission, increases in intensity when the active site is at its closest to the subsolar point and receives maximum Solar heating, and decreases when the active site is farthest from the subsolar point and it receives somewhat diminished Solar heating, assuming the rotational pole is not directed exactly at the Sun.

Given Scheila’s rotation period of 15.848 hr (Warner 2006; Ishiguro *et al.* 2011a), this scenario would require Scheila to have thermal inertia low enough for the temperature of the active site to vary enough during each rotation such that the dust production rate of the jet visibly varies as the active site rotates into and out of direct Solar heating. This scenario would also require a somewhat fortuitous rotation pole orientation where the angle between the pole and the Sun-object vector is large enough to create significant diurnal temperature variations over the course of a single rotation, but small enough that the projected appearance of a Sunward-pointing hollow cone of ejected material that is then pushed back by radiation pressure is not lost. The thermal and numerical dust modeling required to test this scenario is beyond the scope of this paper. We note, however, that the oblique impact scenario described by Ishiguro *et al.* (2011b) is far simpler than one involving a rotating, diurnally-varying cometary jet oriented exactly in such a way that it mimics the asymmetric Sunward-directed hollow cone of ejected material that otherwise arises naturally in the impact scenario. As such, in the absence of compelling evidence that sublimation must be taking place, we favor that impact scenario as the most plausible explanation for Scheila’s unusual dust emission, and therefore consider it to be the second disrupted asteroid to be discovered, after P/2010 A2.

#### 4.3. MBCs vs. Disrupted Asteroids

New and upcoming all-sky survey facilities like the Panoramic Survey Telescope And Rapid Response System (Pan-STARRS; Kaiser *et al.* 2010) and the Large Synoptic Survey Telescope (LSST; Jones *et al.* 2009), as well as long-running existing surveys like LINEAR, Spacewatch, and the Catalina Sky Survey, are expected to discover many more comet-like objects in the future, some of which may be found to orbit in the main asteroid belt. A natural question to pose, then, is how can we distinguish with any degree of certainty which of these objects are MBCs, where comet-like activity is due to sublimation, and which are disrupted asteroids, where comet-like activity is due to a recent impact?

Unfortunately, a definitive answer to this question does not yet exist. For this reason, Jewitt *et al.* (2011) have taken the approach of designating all comet-like objects with main-belt orbits as MBCs, based on their appearance alone (*i.e.*, using the observational definition of a comet as any solar system object exhibiting mass loss in the form of extended surface brightness features such as a coma or tail). Using this definition, they classify Scheila as an “impact-activated MBC”, agreeing with this work in terms of physical conclusions, if not in terminology. We prefer, however, to retain the physical meaning of a “comet” as an active body whose gas or dust emission is due to the sublimation of volatile ices. As such, we choose to define MBCs as only those comet-like objects with main-belt orbits whose activity is sublimation-driven (ac-

ording to our best judgement), as originally specified in Hsieh & Jewitt (2006), and objects like P/2010 A2 and Scheila, where dust emission is the direct consequence of an impact, as disrupted asteroids.

Of course, imposing the requirement that activity must be sublimation-driven for an object to be considered an MBC implies that we know the underlying cause of apparent activity for every comet-like main-belt object, which is not necessarily always the case (or indeed ever the case, at least not until the first successful gas detection is made).

From a practical standpoint, the development of an unambiguous method of distinguishing sublimation-driven dust emission and impact-driven dust emission will require the discovery and thorough individual investigations of many more examples of both types of objects before a set of reliable criteria can be developed for each, meaning that significant additional work is required before such a classification system can be achieved.

In the meantime, we can draw the following preliminary conclusions and observations regarding the differences between MBCs and disrupted asteroids, based on the currently extremely limited populations of each:

1. *Long-lived activity is not a reliable indicator of a dust emission event’s source.* All five currently recognized MBCs exhibited activity persisting over weeks or months (Hsieh *et al.* 2004, 2009, 2011a; Jewitt *et al.* 2009; Moreno *et al.* 2011a), but so did the two currently recognized disrupted asteroids (Jewitt *et al.* 2010, 2011; Snodgrass *et al.* 2010). Long-lived activity in the five recognized MBCs is regarded as an indication of continuous emission over an extended period of time, a characteristic of cometary emission. However, similar long-lived “activity” (>1 month), or rather the persistent presence of a dust cloud, in P/2010 A2 and Scheila are explained as a consequence of the impact events on each object ejecting large ( $\gg 1 \mu\text{m}$ ) particles, which simply take longer to dissipate than smaller particles (Jewitt *et al.* 2010; Bodewits *et al.* 2011).

Observations showing steadily increasing quantities of dust during long-lived active episodes (*e.g.*, for 238P; Hsieh *et al.* 2011b) could be better indications of sublimation-driven activity since they cannot simply be explained by persistent large dust grains. Ongoing dust particle production is required. However, while this can result from the actual release of new dust from the nucleus, an increase in visible scattering surface area could also arise via fragmentation of existing dust particles, as likely occurred during Comet 17P/Holmes’s 2007 outburst (Hsieh *et al.* 2010).

In the case of Scheila, Jewitt *et al.* (2011) argued that observations of rapid fading of the dust cloud (approximately one month after its discovery) was an indication of impact-driven emission. While the short time between the appearance of Scheila’s dust cloud (in December 2010) and this rapid fading (observed in January 2011) means that this interpretation is likely correct, we note that decreasing activity (with no earlier observations of increasing activity) was also observed for 133P in 2002

(Hsieh *et al.* 2004) and P/Garradd in 2008 (Jewitt *et al.* 2009). Thus, while increasing activity may suggest cometary emission, and decreasing activity may suggest impact-driven emission, neither should be considered conclusive proof of either scenario without other supporting evidence.

2. *Dust clouds with unusual morphologies may indicate unusual formation circumstances.* As discussed in Section 4.2 (and references within) for Scheila and by Jewitt *et al.* (2010) and Snodgrass *et al.* (2010) for P/2010 A2, the unusual structures of their respective dust clouds appear to be indications of non-sublimation-driven origins. In the case of P/2010 A2, an observed gap between the nucleus and the dust tail strongly suggested that a dust cloud had been ejected in a single impulsive event and was slowly drifting away from the nucleus, consistent with being an ejecta cloud produced by an impact, and inconsistent with cometary dust emission. The implications of Scheila’s pair of dust plumes are considered at length in Section 4.2. While such interpretations can be used to draw preliminary conclusions, we caution against relying solely on morphology-based determinations of a dust emission event’s source. Multi-tail structures have been observed for comets believed to exhibit sublimation-driven activity (*e.g.*, 238P and P/La Sagra; Hsieh *et al.* 2009; Moreno *et al.* 2011a) and the abrupt termination of sublimation-driven dust emission that could cause an observable gap between a nucleus and a dust tail, while probably uncommon, could be possible given certain topographical circumstances (*e.g.*, shadowing of isolated active sites). Detailed numerical dust modeling must be employed to ensure that any unusual morphological structures cannot be plausibly explained by both sublimation-driven and impact-driven dust emission.
3. *Recurrent activity, separated by intervening periods of inactivity, is extremely difficult to explain as the consequence of impacts.* Upon the initial discovery of a comet-like main-belt asteroid, conclusions about the nature of its activity have generally been the result of numerical dust modeling (Boehnhardt *et al.* 1996; Hsieh *et al.* 2004, 2009, 2011a; Moreno *et al.* 2011a). The underconstrained nature of these modeling efforts, however, means their solutions are usually never unique, and simply reflect the most plausible ejection scenarios as judged by the authors of those studies.

In contrast, observations of recurrent activity for a single object leave far less room for ambiguity (*cf.* 133P and 238P; Hsieh *et al.* 2004, 2010, 2011b). In those cases, repeated active episodes occurred on timescales of  $\sim 5$ -6 years, which correspond closely to the orbital period of each object, and are far shorter than the expected timescales of repeated random collisions on individual main-belt objects by impactors of appreciable size (*e.g.*, Farinella & Davis 1992). One might envision a scenario in which a main-belt object routinely encounters an overdensity of impactors at certain parts of its or-

bit, perhaps due to an intersecting cometary debris stream, for example. The contrived nature of such a scenario (in which debris streams dense enough to reliably impact 133P and 238P on each orbital passage only intersect these specific objects and do not cause comparable events on other asteroids with similar orbits) argues strongly against its plausibility though. On the other hand, repeated active episodes are routinely observed for comets for which activity is driven by sublimation, and can be naturally explained for the MBCs as the consequence of seasonal variations in solar heating of isolated active sites, or perhaps simply from the increase in solar heating experienced by each object near perihelion (Hsieh *et al.* 2004, 2011b).

As discussed above, the sizes of the known populations of both MBCs and disrupted asteroids, from which these generalizations are drawn, are extremely small, and so the typical caveats associated with small-number statistics certainly apply. However, for the above reasons, we suggest that repeated activity is the least ambiguous and most reliably obtainable indicator available at the current time that comet-like activity is sublimation-driven for a particular object. While only two of the seven currently known comet-like main-belt objects (*i.e.*, both MBCs and disrupted asteroids) have been observed to exhibit recurrent activity to date, we note that the remaining five objects were discovered as comet-like bodies recently enough that they have not actually yet completed full orbits since their respective discoveries. As such, continued monitoring of all of these objects to search for recurrent activity will be important for validating their identification as MBCs or disrupted asteroids.

## 5. SUMMARY

We have conducted a photometric, spectroscopic, and dynamical study of comet-like main-belt asteroid (596) Scheila, and report the following findings:

- Scheila’s dust cloud comprises a  $V$ -band photometric excess of  $\Delta = 0.96$  mag over the expected quiescent brightness of the nucleus, giving it a scattering cross-section  $\sim 1.4$  times larger than that of the nucleus, and an estimated total mass of  $M_D \sim 3 \times 10^7$  kg. Separate  $V - R$  color measurements of each of the two curved plumes of the dust cloud show that they are both redder than the Sun, with no significant color differences between the plumes themselves.
- We find no evidence of CN emission in Scheila’s dust cloud down to the sensitivity level of our spectroscopic observations, and place upper limits to CN and  $H_2O$  production rates of  $Q_{CN} = 8.91 \times 10^{23} \text{ s}^{-1}$  and  $Q_{H_2O} \sim 10^{27} \text{ s}^{-1}$ .
- An analysis of Scheila and its dynamical vicinity using numerical simulations indicate that it is dynamically stable for  $> 100$  Myr, suggesting that it is likely native to its current location. We also find that it does not belong to a dynamical asteroid family of any significance, meaning that it is unlikely to be the product of a recent fragmentation or cratering event that could have exposed deeply buried ice.

Considering the available evidence obtained by us and others, we conclude that Scheila is most likely a disrupted asteroid, and not an MBC (where dust emission is the result of the sublimation of ice, as in other comets), in agreement with previous work. This conclusion is largely founded on consideration of the unusual morphology of Scheila's dust cloud, coupled with the simplicity of the impact scenario required to reproduce it and the inability of any physically plausible sublimation-driven scenarios to do likewise. While the currently known examples of MBCs and disrupted asteroids suggest that morphological analyses can provide strong indications as to the nature of comet-like activity in main-belt objects discovered in the future, we caution against relying on such evidence on its own. We suggest instead that recurrence (or absence of recurrence) of comet-like activity is the best indicator available to date of whether an object is likely to be a MBC or a disrupted asteroid, underscoring

the importance of long-term monitoring observations of these objects.

H.H.H. is supported by NASA through Hubble Fellowship grant HF-51274.01, awarded by the Space Telescope Science Institute, operated by the Association of Universities for Research in Astronomy, Inc., for NASA, under contract NAS 5-26555. B.Y. and N.H. acknowledge support through the NASA Astrobiology Institute under Cooperative Agreement No. NNA08DA77A issued through the Office of Space Science. We thank Carl Hergenrother for first alerting us to Scheila's unusual activity, Anthony Readhead, Roger W. Romani, and Joseph L. Richards for obtaining Keck observations for us, Marc Kassiss and Richard Morriarty for technical assistance, David Nesvorný for providing hierarchical clustering analysis software, David Jewitt, Masateru Ishiguro, and Iwan Williams for valuable discussions, and an anonymous referee for helpful comments on this manuscript.

## REFERENCES

- A'Hearn, M. F. 1982, IAU Colloq. 61: Comet Discoveries, Statistics, and Observational Selection, 433
- A'Hearn, M. F., Millis, R. L., Schleicher, D. G., Osip, D. J., & Birch, P. V. 1995, *Icarus*, 118, 223
- Bagnulo, S., Tozzi, G. P., Boehnhardt, H., Vincent, J.-B., & Muinonen, K. 2010, *A&A*, 514, A99.
- Beck, P., Quirico, E., Sevestre, D., Montes-Hernandez, G., Pommerol, A., & Schmitt, B. 2011, *A&A*, 526, A85.
- Binzel, R. P., & Xu, S. 1993, *Science*, 260, 186
- Biver, N., et al. 1997, *Earth Moon and Planets*, 78, 5
- Bodewits, D., Kelley, M. S., Li, J.-Y., Landsman, W. B., Besse, S., & A'Hearn, M. F. 2011, *ApJ*, 733, L3
- Boehnhardt, H., Schulz, R., Tozzi, G. P., Rauer, H., & Sekanina, Z. 1996, *IAU Circ.*, 6495, 2
- Bottke, W. F., Jr., Vokrouhlický, D., Rubincam, D. P., & Broz, M. 2002, *Asteroids III*, 395
- Bottke, W. F., Durda, D. D., Nesvorný, D., Jedicke, R., Morbidelli, A., Vokrouhlický, D., & Levison, H. F. 2005, *Icarus*, 179, 63
- Campins, H., Hargrove, K., Pinilla-Alonso, N., Howell, E. S., Kelley, M. S., Licandro, J., Mothé-Diniz, T., Fernández, Y. R., & Ziffer, J. 2010, *Nature*, 464, 1320-1321.
- Chambers, J. E. 1999, *MNRAS*, 304, 793
- Elst, E. W., Pizarro, O., Pollas, C., Ticha, J., Tichy, M., Moravec, Z., Offutt, W., & Marsden, B. G. 1996, *IAUC* 6496
- Farinella, P., & Davis, D. R. 1992, *Icarus*, 97, 111
- Farinella, P., Vokrouhlický, D., & Hartmann, W. K. 1998, *Icarus*, 132, 378
- Fernández, J. A., Gallardo, T., & Brunini, A. 2002, *Icarus*, 159, 358
- Finson, M. L., & Probst, R. F. 1968, *ApJ*, 154, 327
- Fitzsimmons, A., Dahlgren, M., Lagerkvist, C.-I., Magnusson, P., & Williams, I. P. 1994, *A&A*, 282, 634
- Fornasier, S., Dotto, E., Hainaut, O., Marzari, F., Boehnhardt, H., de Luise, F., & Barucci, M. A. 2007, *Icarus*, 190, 622
- Haghighipour, N. 2009, *Meteoritics and Planetary Science*, 44, 1863
- Haser, L. 1957, *Bulletin de la Societe Royale des Sciences de Liege*, 43, 740
- Hildebrand, A. R., McCausland, P. J. A., Brown, P. G., Longstaffe, F. J., Russell, S. D. J., Tagliaferri, E., Wacker, J. F., & Mazur, M. J. 2006, *Meteoritics & Planetary Science*, 41, 407
- Howell, E. S., & Lovell, A. J. 2011, *IAU Circ.*, 9191, 2
- Hsieh, H. H., Jewitt, D., & Fernández, Y. R. 2004, *AJ*, 127, 2997
- Hsieh, H. H., & Jewitt, D. 2006, *Science*, 312, 561
- Hsieh, H. H. 2009, *A&A*, 505, 1297
- Hsieh, H. H., Jewitt, D., & Ishiguro, M. 2009, *AJ*, 137, 157
- Hsieh, H. H., Fitzsimmons, A., Joshi, Y., Christian, D., & Pollacco, D. L. 2010a, *MNRAS*, 407, 1784-1800
- Hsieh, H. H., Jewitt, D., Lacerda, P., Lowry, S. C., & Snodgrass, C. 2010b, *MNRAS*, 403, 363-377
- Hsieh, H. H., Ishiguro, M., Lacerda, P., & Jewitt, D. 2011a, *AJ*, 142, 29
- Hsieh, H. H., Meech, K. J., & Pittichová, J. 2011b, *ApJ*, 736, L18
- Ishiguro, M., Hanayama, H., Hasegawa, S., Sarugaku, Y., Watanabe, J., Fujiwara, H., Terada, H., Hsieh, H. H., Vaubaillon, J. J., Kawai, N., Yanagisawa, K., Kuroda, D., Miyaji, T., Fukushima, H., Ohta, K., Hamanowa, H., Kim, J., Pyo, J., & Nakamura, A. M. 2011a, *ApJ*, in press
- Ishiguro, M., Hanayama, H., Hasegawa, S., Sarugaku, Y., Watanabe, J., Fujiwara, H., Terada, H., Hsieh, H. H., Vaubaillon, J. J., Kawai, N., Yanagisawa, K., Kuroda, D., Miyaji, T., Fukushima, H., Ohta, K., Hamanowa, H., Kim, J., Pyo, J., & Nakamura, A. M. 2011b, *ApJ*, submitted
- Jehin, E., Manfroid, J., Hutsemekers, D., Gillon, M., & Magain, P. 2011, *Central Bureau Electronic Telegrams*, 2632, 2
- Jewitt, D. 2009, *AJ*, 137, 4296-4312.
- Jewitt, D., Yang, B., & Haghighipour, N. 2009, *AJ*, 137, 4313
- Jewitt, D., Weaver, H., Agarwal, J., Mutchler, M., & Drahus, M. 2010, *Nature*, 467, 817
- Jewitt, D., Weaver, H., Mutchler, M., Larson, S., & Agarwal, J. 2011, *ApJ*, 733, L4
- Jones, T. D., Lebofsky, L. A., Lewis, J. S., & Marley M. S. 1990, *Icarus*, 88, 172
- Jones, R. L., et al. 2009, *Earth Moon and Planets*, 105, 101
- Kaiser, N., et al. 2010, *Proc. SPIE*, 7733,
- Knežević, Z., & Milani, A. 2003, *A&A*, 403, 1165
- Landolt, A. U. 1992, *AJ*, 104, 340
- Larson, S. M. 2010, *IAU Circ.*, 9188, 1
- Licandro, J., Campins, H., Kelley, M., Hargrove, K., Pinilla-Alonso, N., Cruikshank, D., Rivkin, A. S., & Emery J. 2011, *A&A*, 525, A34
- Licandro, J., Campins, H., Tozzi, G. P., De León, J., Pinilla-Alonso, N., Boehnhardt, H., Hainaut, O. R. 2011, *A&A*, 532, A65
- Meech, K. J., et al. 2011, *Icarus*, 213, 323
- Moreno, F., Licandro, J., Tozzi, G.-P., Ortiz, J. L., Cabrera-Laver, A., Augustejn, T., Liimets, T., Lindberg, J. E., Pursimo, T., Rodríguez-Gil, & Vaduvescu, O. 2010, *ApJ*, 718, L132
- Moreno, F., Lara, L. M., Licandro, J., Ortiz, J. L., De León, J., Alí-Lagoa, V., Agis-González, B., & Molina, A. 2011a, *ApJ*, 738, L16.
- Moreno, F., Licandro, J., Ortiz, J. L., Lara, L. M., Alí-Lagoa, V., Vaduvescu, O., Morales, N., Molina, A., & Lin, Z.-Y. 2011b, *ApJ*, 738, 130
- Nakamura, T., & Yoshikawa, M. 1993, *Celestial Mechanics and Dynamical Astronomy*, 57, 113
- Nesvorný, D., Jedicke, R., Whiteley, R. J., Ivezić, Ž. 2005, *Icarus*, 173, 132

TABLE 1  
OBSERVATION LOG

UT Date	Telescope	Obs. <sup>a</sup>	$N^b$	$t^c$	Filters	$\theta_s^d$	$\nu^e$	$r_n^f$	$\Delta^g$	$\alpha^h$	$\alpha_{pl}^i$
2010 Dec 12	UH 2.2m	Im	81	1770	<i>V</i>	0''8	239.6	3.107	2.529	16.4	-1.0
2010 Dec 12	UH 2.2m	Im	97	2230	<i>R</i>	0''8	239.6	3.107	2.529	16.4	-1.0
2010 Dec 17	Keck I	Sp	2	1800	—	1''0	240.5	3.100	2.462	15.6	-1.5

<sup>a</sup> Type of observation (Im: imaging; Sp: spectroscopy)

<sup>b</sup> Number of images

<sup>c</sup> Total effective exposure time in seconds

<sup>d</sup> FWHM seeing in arcsec

<sup>e</sup> True anomaly in arcsec

<sup>f</sup> Heliocentric distance in AU

<sup>g</sup> Geocentric distance in AU

<sup>h</sup> Solar phase angle in degrees

<sup>i</sup> Orbit plane angle (between the observer and object orbit plane as seen from the object) in degrees

TABLE 2  
NUCLEUS AND DUST PHOTOMETRY

	$m_V$	$m_R$	$V - R$
Nucleus <sup>a</sup>	14.22±0.01	13.77±0.01	0.45±0.02
Total <sub>A</sub> <sup>b</sup>	13.73±0.02	13.27±0.02	0.45±0.03
Dust <sub>A</sub> <sup>c</sup>	14.84±0.02	14.36±0.02	0.48±0.03
Dust <sub>B</sub> <sup>d</sup>	22.79±0.03	22.78±0.03	0.51±0.04
Dust <sub>C</sub> <sup>e</sup>	23.43±0.04	23.00±0.04	0.43±0.06

<sup>a</sup> Photometry of nucleus (including unresolved near-nucleus coma) inside a 3''0 (radius) circular photometry aperture

<sup>b</sup> Photometry of nucleus and dust inside aperture "A" as marked in Figure 2

<sup>c</sup> Nucleus-subtracted photometry of dust inside aperture "A" (Fig. 2)

<sup>d</sup> Photometry of dust inside aperture "B" (Fig. 2)

<sup>e</sup> Photometry of dust inside aperture "C" (Fig. 2)

Oke, J. B., Cohen, J. G., Carr, M., Cromer, J., Dingizian, A., Harris, F. H., Labrecque, S., Lucinio, R., Schaal, W., Epps, H., & Miller, J. 1995, *PASP*, 107, 375

Prialnik, D., & Rosenberg, E. D. 2009, *MNRAS*, 399, L79

Read, M. T., Bressi, T.H., Gehrels, T., Scotti, J. V., & Christensen, E. J. 2005, *IAU Circ.*, 8624, 1

Richardson, J. E., Melosh, H. J., Lisse, C. M., & Carcich, B. 2007, *Icarus*, 190, 357

Rousselot, P., Dumas, C., & Merlin, F. 2011, *Icarus*, 211, 553-558.

Rivkin, A. S., & Emery, J. P. 2010, *Nature*, 464, 1322-1323.

Schleicher, D. G. 2010, *AJ*, 140, 973

Schorghofer, N. 2008, *ApJ*, 682, 697

Snodgrass, C., Tubiana, C., Vincent, J.-B., Sierks, H., Hviid, S., Moissi, R., Boehnhardt, H., Barbieri, C., Koschny, D., Lamy, P., Rickman, H., Rodrigo, R., Carry, B., Lowry, S. C., Laird, R. J. M., Weissman, P. R., Fitzsimmons, A., Marchi, S., & The Osiris Team. 2010, *Nature*, 467, 814

Tedesco, E. F., Noah, P. V., Noah, M., & Price, S. D. 2004, IRAS Minor Planet Survey, IRAS-A-FPA-3-RDR-IMPS-V6.0. NASA Planetary Data System.

Thomas, P. C., Binzel, R. P., Gaffey, M. J., Storrs, A. D., Wells, E. N., Zellner, B. H. 1997, *Science*, 277, 1492

Warner, B. D. 2006, *Minor Planet Bulletin*, 33, 58

Warner, B., Harris, A. W., Nakano, S., Yoshimoto, K., Guido, E., Nevski, V., Yusa, T., Foglia, S., Buzzi, L., Concari, P., Galli, G., Tombelli, M., Bryssinck, E., & Gonzalez, J. J. 2010, *Central Bureau Electronic Telegrams*, 2590, 1

Yang, B., & Hsieh, H. H. 2011, *ApJ*, 737, L39

Zappalà, V., Cellino, A., Farinella, P., & Knežević, Z. 1990, *AJ*, 100, 2030

Zappalà, V., Cellino, A., Farinella, P., & Milani, A. 1994, *AJ*, 107, 772

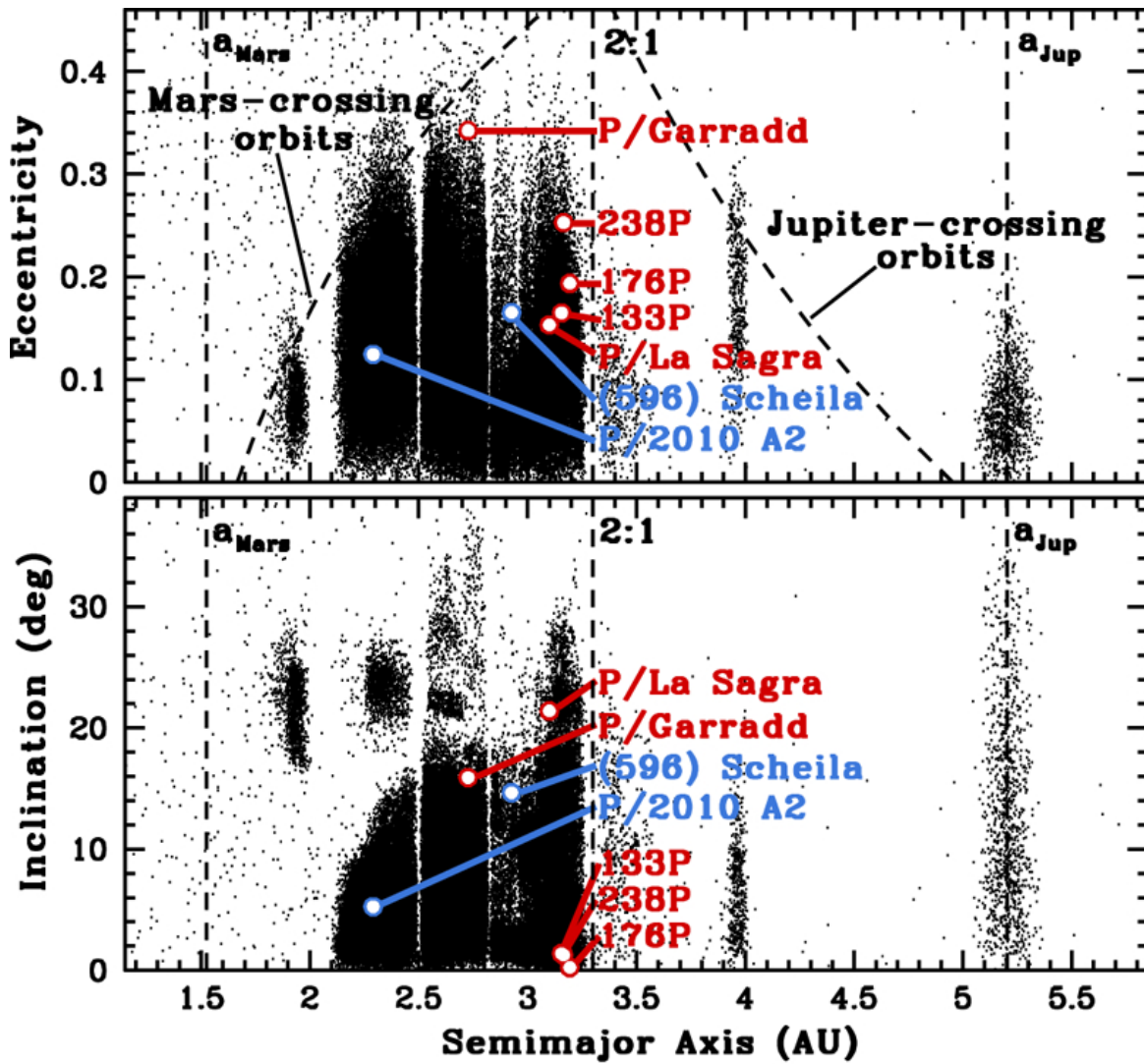


FIG. 1.— Plots of eccentricity (top) and inclination (bottom) versus semimajor axis showing the distributions in orbital element space of main-belt asteroids (black dots), main-belt comets (red circles), and likely disrupted asteroids P/2010 A2 and Scheila (blue circles). Also marked with dotted lines are the semimajor axes of Mars ( $a_{\text{Mars}}$ ) and Jupiter ( $a_{\text{Jup}}$ ), the semimajor axis of the 2:1 mean-motion resonance with Jupiter, and the loci of Mars-crossing orbits and Jupiter-crossing orbits.

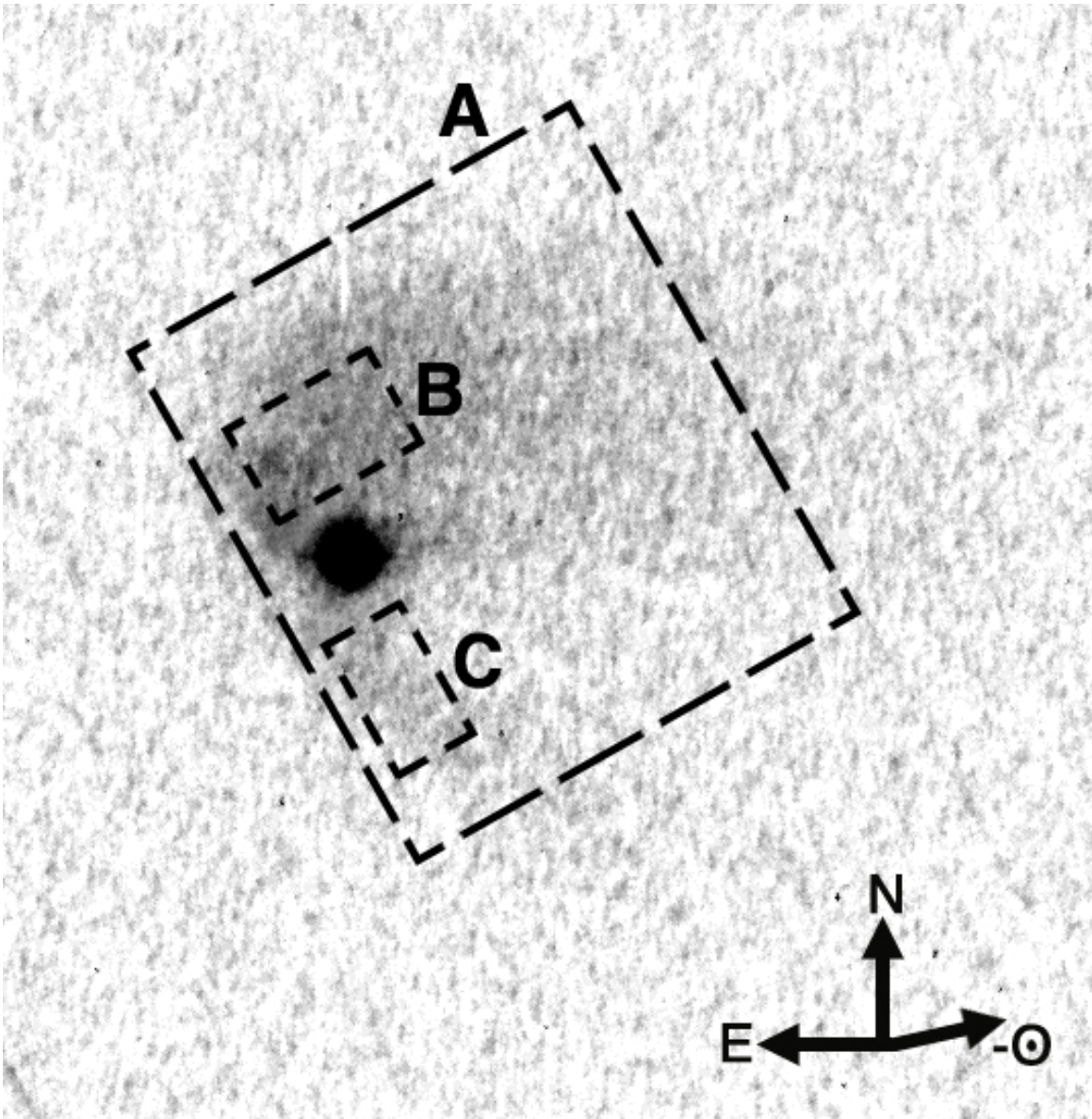


FIG. 2.— Composite *R*-band image of Scheila constructed from data obtained using the UH 2.2 m telescope on 2010 December 12 and comprising data equivalent to 2230 s in total exposure time. Rectangular photometry apertures used to measure dust fluxes are marked, where aperture “A” is  $53'' \times 62''$  in size, “B” is  $17''.5 \times 11''.0$ , and “C” is  $9''.2 \times 15''.9$ .

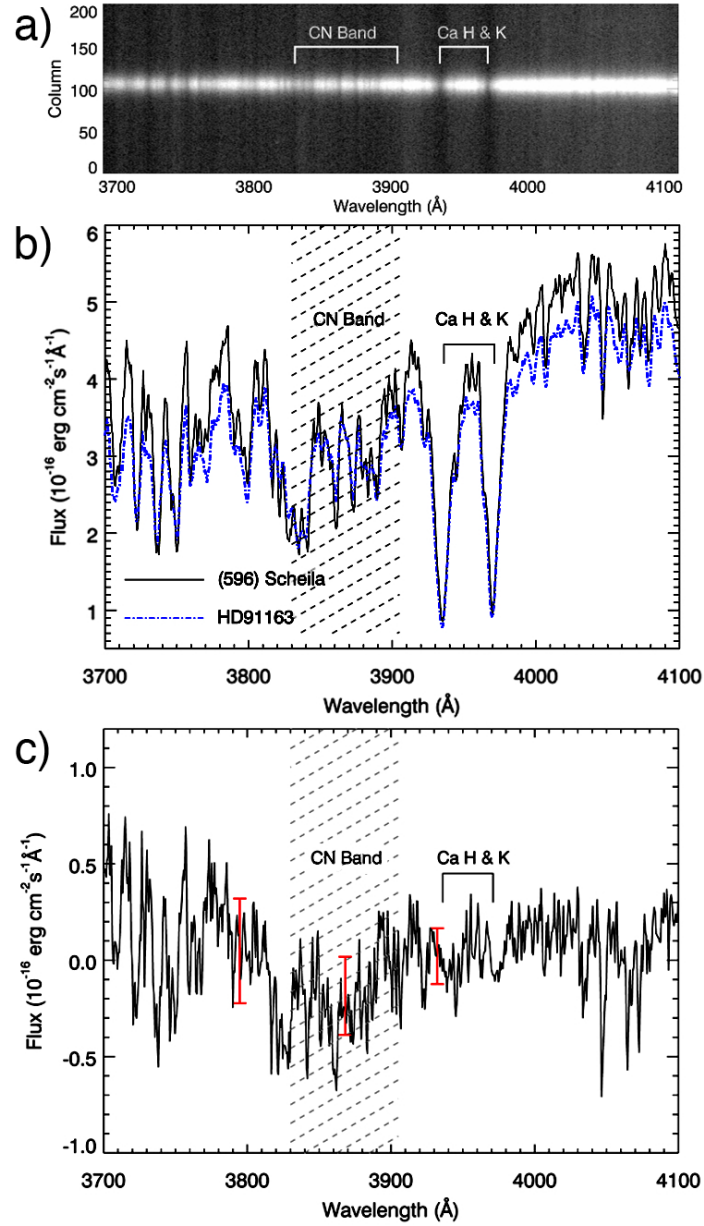


FIG. 3.— (a) Long slit spectral image of Scheila, taken on UT 2010 December 17 using Keck I. The wavelength range ( $3830\text{Å} < \lambda < 3905\text{Å}$ ) where CN emission is expected is marked. Sky emission lines are visible along the spatial direction (the vertical axis) and the solar Ca H and K absorption lines are marked. (b) Sky background-subtracted and flux-calibrated spectrum of Scheila (solid black line). The scaled spectrum of the solar analog, G2V star HD 91163, is marked as a blue dashed line. The shaded region indicates where CN emission is expected. (c) Spectrum of Scheila with the underlying solar-type continuum subtracted. Red error bars show the  $1\sigma$  uncertainties in the three wavelength regions discussed in the text.

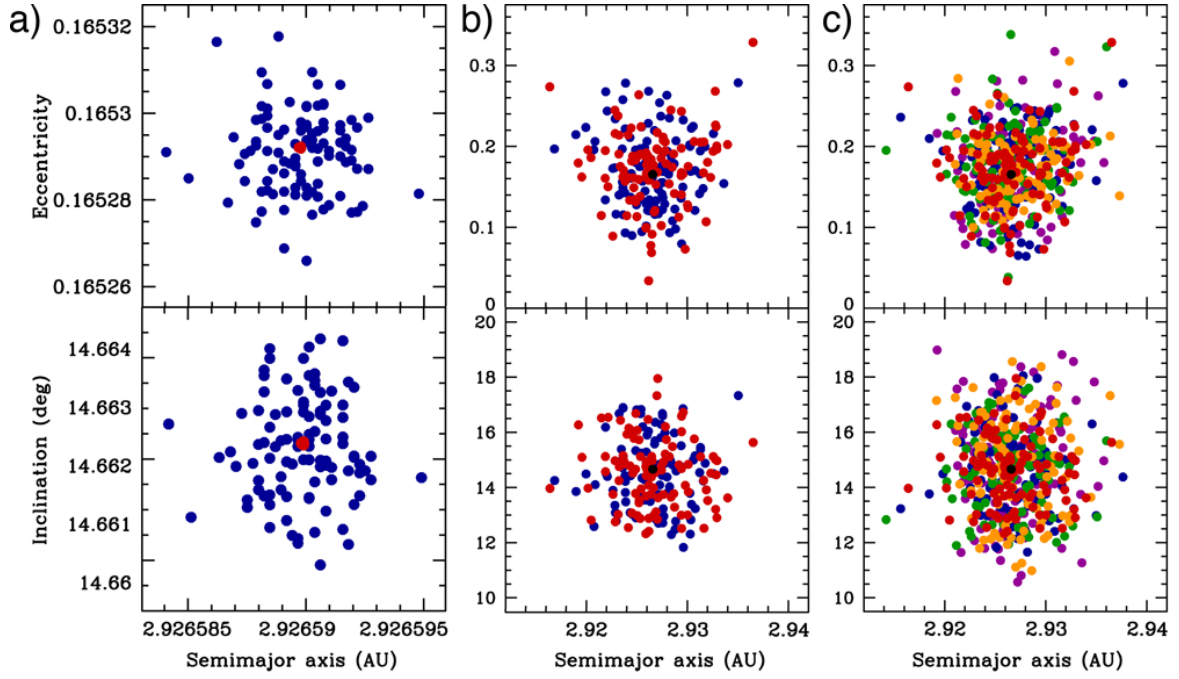


FIG. 4.— Plots of semimajor axis versus eccentricity (top) and inclination (bottom) for (a) the initial orbital elements and (b) final orbital elements after a 100 Myr dynamical integration of 100  $1\text{-}\sigma$  Scheila test particles (red dots) and 100  $100\text{-}\sigma$  test particles (blue dots), and (c) the orbital elements of the same 100  $1\text{-}\sigma$  test particles shown at the start of our simulation (overlapping black dots at the center of each panel) and 100  $1\text{-}\sigma$  test particles after 20 Myr (purple), 40 Myr (blue), 60 Myr (green), 80 Myr (orange), and 100 Myr (red).